Correlation between plant cell wall stiffening and root extension arrest phenotype in the combined abiotic stress of Fe and Al

Harinderbir Kaur, Jean-marie Teulon, Christian Godon, Thierry Desnos, Shu-wen W Chen, Jean-luc Pellequer

Received: 21 February 2023 | Revised: 1 October 2023 | Accepted: 15 October 2023

DOI: 10.1111/pce.14744

ORIGINAL ARTICLE

Plant, Cell & Environment | WILEY

Correlation between plant cell wall stiffening and root extension arrest phenotype in the combined abiotic stress of Fe and Al

Harinderbir Kaur[1] | Jean-Marie Teulon[1] | Christian Godon[2] | Thierry Desnos[2] | Shu-wen W. Chen[1,3] | Jean-Luc Pellequer[1]

[1]Univ. Grenoble Alpes, CEA, CNRS, IBS, Grenoble, France

[2]Aix Marseille Université, CEA, CNRS, BIAM, Saint Paul-Lez-Durance, Cadarache, France

[3]Rue Cyprien Jullin, Vinay, France

Correspondence
Jean-Luc Pellequer, Institut de Biologie Structurale, Grenoble, 38000, France.
Email: Jean-luc.pellequer@ibs.fr

Funding information
Agence Nationale de la Recherche; European Union's Horizon 2020 research and innovation programme, Grant/Award Number: 812772

Abstract

The plasticity and growth of plant cell walls (CWs) remain poorly understood at the molecular level. In this work, we used atomic force microscopy (AFM) to observe elastic responses of the root transition zone of 4-day-old *Arabidopsis thaliana* wild-type and *almt1*-mutant seedlings grown under Fe or Al stresses. Elastic parameters were deduced from force-distance curve measurements using the trimechanic-3PCS framework. The presence of single metal species Fe^{2+} or Al^{3+} at 10 µM exerts no noticeable effect on the root growth compared with the control conditions. On the contrary, a mix of both the metal ions produced a strong root-extension arrest concomitant with significant increase of CW stiffness. Raising the concentration of either Fe^{2+} or Al^{3+} to 20 µM, no root-extension arrest was observed; nevertheless, an increase in root stiffness occurred. In the presence of both the metal ions at 10 µM, root-extension arrest was not observed in the *almt1* mutant, which substantially abolishes the ability to exude malate. Our results indicate that the combination of Fe^{2+} and Al^{3+} with exuded malate is crucial for both CW stiffening and root-extension arrest. However, stiffness increase induced by single Fe^{2+} or Al^{3+} is not sufficient for arresting root growth in our experimental conditions.

KEYWORDS
atomic force microscopy (AFM), elasticity, nanoindentation, primary root, trimechanic-3PCS

1 | INTRODUCTION

The cell wall (CW) of land plants has been depicted as a highly intertwining architecture consisting of cellulose microfibrils, hemicellulose and pectin (Carpita & Gibeaut, 1993), which compose the three major components of the primary CW. Cellulose microfibrils are the stiffest component, playing a load-bearing role (Bashline et al., 2014; Bidhendi & Geitmann, 2016; Cosgrove, 2005, 2018). Their orientation creates a mechanical anisotropy, restricting cell expansion in the microfibril direction (Majda et al., 2017). Hemicelluloses (xyloglucan chains) bind to cellulose microfibrils using hydrogen bonds (Valent & Albersheim, 1974); they also bind covalently to pectin (Bauer et al., 1973), a network made of matrix pectin polysaccharides and soluble proteins (Kerr & Bailey, 1934). Water is also a major constituent of primary CWs (Gaff & Carr, 1961), up to 65% (Jackman & Stanley, 1995), and an essential element for

chemical reactions within the CW. The thickness of the primary CW was suggested to be around 80–100 nm for meristematic and parenchymatous cells, in accordance with a layered structure of cellulose microfibrils with a layer spacing of ~20–40 nm (McCann et al., 1990). However, the accurate thickness measurement of external primary CWs remains challenging, roughly estimated as ~0.1–1 µm (Derbyshire et al., 2007).

Cell growth is characterized by an irreversible increase in cell volume and surface area, concomitant with a CW loosening. The complexity of CW growth results in poorly known pathways and mechanisms that control root CW plasticity (Somssich et al., 2016). Upon various environmental stresses, a reduction of cell growth associated with CW stiffening is a well-known phenomenon observed in plants (Schopfer, 2006), tightly linked to dynamic behaviours of primary CWs. It has been proposed that strain-stiffening limits growth and restricts organ bulging (Kierzkowski et al., 2012). During plant growth, some cells enlarge their volumes by 10–1000 times (Cosgrove, 1997), with this growth regulated by external stimuli such as temperature, light, water, xenobiotics and internal factors like growth hormones (Preston & Hepton, 1960). The cessation of coleoptile growth was attributed to the loss of CW plasticity but not to turgor pressure which implicates an increase of CW stiffness (Kutschera, 1996). One pioneering work on CW nanomechanics used atomic force microscopy (AFM) to observe stiffness heterogeneity in the meristem surfaces at regional, cellular and even subcellular levels (Milani et al., 2011). AFM has been shown to be powerful for stiffness measurements on plant tissues (Cuadrado-Pedetti et al., 2021; Milani et al., 2014; Peaucelle et al., 2011). For characterizing the nano-stiffness of a sample in response to a given stress, AFM nanoindentation provides a promising strategy of detecting changes in physico-chemical properties of cellular or tissue surfaces on a nanoscale.

Recently, stiffening of seedling roots has been observed within 30 min after exposition to iron stress (Balzergue et al., 2017). In a condition of low phosphate, low pH (<6) and the presence of iron, a primary root extension arrest (REA) was observed and a signalling pathway involving STOP1 and ALMT1 proteins was found to inhibit CW expansion (Balzergue et al., 2017; Mora-Macias et al., 2017). STOP1 abundance in the nucleus of the plant cell was found to be controlled by the presence of iron (Fe) and aluminum (Al) metals, both of which induced malate exudation through the ALMT1 channel (Godon et al., 2019; Le Poder et al., 2022). Although Fe is a fundamental nutrient for plants, a defense mechanism somehow occurs in a Fe-rich environment, implying that an excess of Fe is deleterious to plants (Oliveira de Araujo et al., 2020). The deleterious effect of Fe is linked with the ferritin capacity of plant cell for storing free reactive iron (Ravet et al., 2009) instead of being driven to the vacuole (Hirsch et al., 2006; Ward et al., 2008). Indeed, ferritin encapsulates the Fe^{3+} cation after oxidizing Fe^{2+} before storage (Macara et al., 1972). In bean roots, the apoplast provides a storage space for Fe^{3+}, where it could be extracted for nutrition use in case of iron deficiency (Bienfait et al., 1985). The *Arabidopsis lpr1/lpr2* mutants lack the capability of oxidizing Fe^{2+} to Fe^{3+} and were shown to reduce the amount of iron in the apoplast, exhibiting a Fe-insensitive phenotype in low-phosphate conditions (Svistoonoff et al., 2007).

Inhibition of root elongation is a well-known plant response to the tolerance of Al (Clarkson, 1965), especially at low pH (Bian et al., 2013). Al toxicity resides in its cationic binding to negatively charged sites (membranes, proteins, saccharides) available in the root (Nichol et al., 1993). One creep-extension analysis showed that Al accumulation in the CW provoked a reduction of CW extensibility in wheat roots (Ma et al., 2004). Within 1 h of Al supply, callose deposition was observed in the root tip of soybean seedlings (Wissemeier et al., 1992). In addition to callose deposition, the main physiological mechanism of Al tolerance is the exclusion of Al from the root apex (Kochian et al., 2015), where Al usually accumulates in the root apex symplast and the apoplast (Delhaize & Ryan, 1995) and binds directly to negatively charged pectins of the CW of root border cells (Yang et al., 2016). This exclusion is accomplished by exudation of organic acids (Miyasaka et al., 1991) such as malate and citrate (Liu et al., 2009). In cultured tobacco, Al accumulation in plant cell walls was found to depend on the presence of ferrous iron (Fe^{2+}) (Chang et al., 1999). However, unlike Al, Fe does not stimulate malate excretion (Delhaize et al., 1993).

Fe^{2+} in phosphate-deficient conditions is able to arrest primary root growth (Abel, 2011; Godon et al., 2019). Potential harmfulness of excessive Fe to cells is attributed to ROS (reactive oxygen species) production either by the Fenton (involving Fe^{2+}) or by the Haber-Weiss reactions (Fe^{3+}) (Gill & Tuteja, 2010). Concentration above 40 µM of mixed Fe with Al resulted in a drastic reduction of root length, likely through the ROS production (Cakmak & Horst, 1991). The presence of Fe^{2+} in *Arabidopsis* roots stimulates ROS production with peroxidase activity (Balzergue et al., 2017; Müller et al., 2015; Naumann et al., 2022), particularly together with the class III peroxidase to stiffen and loosen the plant CWs (Francoz et al., 2015; Passardi et al., 2005; Wolf & Hofte, 2014). In grass, peroxidase activity was linked to leaf growth arrest and CW cross-linking (MacAdam & Grabber, 2002); in rice, peroxidase was found to be present in coleoptile growth arrest of shoots with increased ferulic and diferulic acids (Wakabayashi et al., 2012); similar findings were obtained for maize (Uddin et al., 2014). However, the causality between CW stiffness and REA remains to be elucidated.

To investigate Al and Fe effects on physiology and morphology of growing roots, we performed AFM indentations on *Arabidopsis* seedling roots under Fe and Al stresses using various metal concentrations and compositions. The present research provides a link between measurements of the structural stiffness (Chen et al., 2023) with stress effects of metal ions on root growth. The recently developed trimechanic-3PCS framework was used throughout this study (Chen et al., 2023). The correspondence between the variations in the magnitude of elasticity parameters and the length of seedling roots under these stress conditions, our understanding of the molecular mechanisms of CW stiffening and root growth as a function of metal ion concentration can be improved.

2 | MATERIALS AND METHODS

2.1 | Seedling growth and manipulation

The experimental specimens are *Arabidopsis thaliana* L. (Heynh.) lines of Columbia (Col-0) or the Col^{er105} background as specified in (Bonnot et al., 2016). The production of $almt1^{51}$ mutant was previously described (Balzergue et al., 2017). Seeds were surface sterilized by 70% ethanol +0.05% SDS for 1 min, followed by washing twice with 95% ethanol for 1 min each time and drying in a laminar airflow hood. To alleviate gravitropism effects on seedling growth such as inducing root wriggling or waving by growing vertically in a Petri dish, the seeds sown on Day 0 were placed in a 24-well crystallization plate (VDX plate HR3-140, Hampton Research). Plates were placed in a growing chamber (IPP100+ incubator; Memmert, Fisher Scientific) for 4 days with a 16-h photoperiod with 24°C/21°C day/night, respectively. During the 4 days, seedlings grew under the −Pi condition (no phosphate added) in the nutrient solution. The chemical content of the agar presently used is particularly poor in phosphate and metals, as determined by ICP analysis (Mercier et al., 2021), which is different from the agar used in our previous study (Balzergue et al., 2017).

After 4 days, seedlings were transferred into 60-mm agar Petri dishes in the −Pi condition while supplemented with or without 10 or 20 µM of $FeCl_2$ and/or $AlCl_3$ for 2 h. Then, seedlings were transferred from the agar plates to a glass slide for AFM nanoindendation experiments and classical force–distance curves were collected within 30 min after mounting the samples on the glass slide. In brief, a thin layer of silicone, NuSil MED1-1356 (NuSil Technology LLC), was spread on the glass slide as described (Kaur, Godon, et al., 2023; Kaur, Teulon, et al., 2023). Partial polymerization was allowed for a few seconds before the root was laid over the silicone. Then, several thin silicone bands were stretched using a syringe needle to fasten the root over all its length except the transition zone, which is located about 500 µm from the root apex (Figure 1). To prevent drying, a droplet of the growth medium (without the agar powder) was deposited to cover the entire seedling. The mounted seedling was positioned under the AFM for data acquisition (Figure 1).

2.2 | Length measurement of primary root

The root lengths were measured on Day 6 after sowing with seedlings directly deposited in the Petri dishes. The photos were taken with a standard phone camera and the root lengths in the photos were measured using the NeuronJ plugin (Meijering et al., 2004) of ImageJ software (Schneider et al., 2012) with a 5 mm grid paper for length calibration. Snapshots from NeuronJ root tracing were saved in the PNG format and data were plotted using GraphPad Prism 5.0.

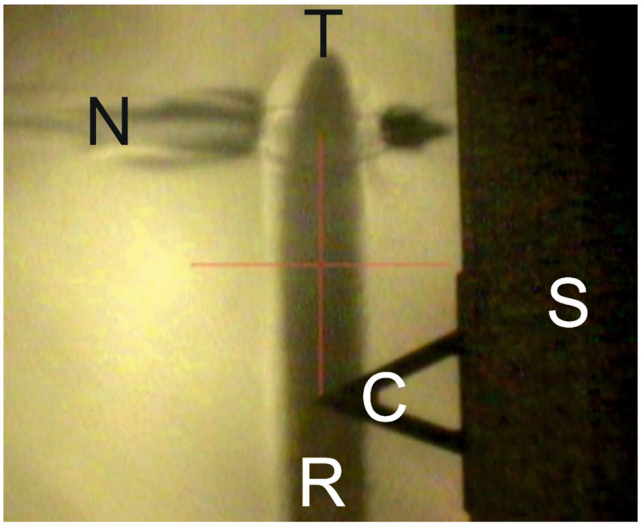

FIGURE 1 Principle of nanomechanical measurement of seedling roots with atomic force microscopy. A seedling root (R) is deposited on a microscope slide using silicon glue (N, for Nusil). A fastening band of silicon is seen near the tip of the root (T). The thickness of the fastening band must be thin enough to avoid hindering the AFM support (S), but thick enough to withstand the bending of the root tip. The root is placed under the AFM cantilever (C) as observed by the AFM optical camera. The triangular shaped cantilever (200 µm long) was placed 500 µm away from the root tip in the transition zone where nanoindentation measurements proceeded (as shown). The seedling root and the AFM cantilever are placed within a liquid environment (growth solution, see Supplementary file). AFM, atomic force microscopy. [Color figure can be viewed at wileyonlinelibrary.com]

2.3 | Nanoindentation experiments with atomic force microscopy

Force–distance (F–D) curves were obtained using an AFM Dimension 3100 (Bruker) with a nanoscope five controller running the Nanoscope 7.3 software. Triangular pyrex nitride cantilever with pyramidal tips of a max nominal radius 10 nm, a half-opening angle of 35°, and a nominal spring constant k = 0.08 N/m were used (PNP-TR; NanoWorld AG).

Calibration of photodiode sensitivity was done first using the approach-retract curve in air on the glass substrate followed by a thermal tuning to determine the cantilever spring constant (Kaur, Teulon, et al., 2023). The determined spring constants were about 0.08 ± 0.01 N/m. In case of a large divergence, the cantilever was manually readjusted inside the probe holder and the calibration was repeated (Schillers et al., 2017). Then the photodiode sensitivity was performed again in a liquid medium with an average value of 65 nm/V. In our case, a SUM value of 3.5–4 V was usually achieved with PNP-TR cantilevers. The engaging deflection setpoint was kept at 2.5 V while the initial vertical deflection on the photodiode was set to 0 V. For performing the indentation experiment, a ramp size of 3 µm, a scan rate of 0.5 Hz, and 4096 data points per curve were set.

Trigger was set off and no trigger value was used, implying that z-start value for the ramp at each new engagement may need adjustments. To limit the maximal force during the measurement, a range of 25–40 nN was usually adopted for F–D data values.

The glass slide with a glued seedling (Figure 1) was positioned under the AFM cantilever with the help of an AFM optical camera. Due to the large motorized sample stage, the glass slide was adjusted in such a way that the cantilever could be positioned perpendicularly at the longitudinal middle of the glued root. The target working area, the transition zone, was 500 µm away from the root apex, almost twice the length of PNP cantilever.

2.4 | Hierarchical statistics and reproducibility of experiments

Owing to the roughness of root surfaces, indentations were performed at various locations in a matrix form. Different sizes of matrices were used: 5 × 2, 4 × 3, 4 × 4, representing 10, 12 or 16 indenting nodes. The optimal distance between nodes was 5 µm. Each node was formed of a submatrix with 3 × 3 or 2 × 2 F–D curves spaced by 50 nm in X and Y directions. Most of the presented results were obtained with a 4 × 4 node matrix of a 2 × 2 submatrix. Measurements from various forms of matrices were merged altogether. It usually took 25 min to record a full set of F–D curves for a single seedling root; the manipulation time was kept as short as possible to avoid additional stress effects.

For each stress condition, experiments were repeated three to five times. Each experiment involved two to four plants. The robustness of our protocol was confirmed by reproducible results from experiments repeated in a remote institute with another AFM instrument (Nanowizard IV, JPK-Bruker). Here, we considered all the measurements on one plant as one independent experiment. To synthesize the overall measurements into one comprehensive result for elasticity of the plant, hierarchical statistics were adopted. Explicitly, each elasticity parameter of one plant was obtained by averaging all the collected data (with 3 × 3 or 2 × 2 submatrices) of a node, then subsequently averaged over all the nodes of the plant. For one stress condition, at least 10 plants were analyzed ($n \geq 10$).

Regarding the reproducibility of results, two criteria were imposed: a valid node should have more than half of its F–D curves within 2 sigma from the mean; a valid plant needs at least half of its measured nodes valid. The distribution of elastic parameters from all nodes of a given stress condition was most often log-normal. Therefore, we computed geometric means for the average value of elastic parameters of a plant. We also applied nonparametric Mann–Whitney *t* tests to evaluating the statistical significance of these parameters among different stress conditions using a null hypothesis that assumes no difference on average among these conditions. A *p* value was calculated using Graphpad Prism 5.0 with an α-threshold of 0.01. The box-and-whiskers plots were drawn using Graphpad Prism 8.

2.5 | Characterization of plant elasticity by the trimechanic-3PCS framework

The trimechanic-3PCS framework (Chen et al., 2023) allows us to investigate the variation of stiffness with varied depth for biomaterials of heterogeneous elasticity responding to an external force. For a depth of indentation trajectory exhibiting a linear-elasticity behaviour, this theory states that the responding force F_T of that depth zone can be expressed as a linear combination of three force components: F_C, F_H and F_S. In this work, the elasticity parameters of the very surface of CWs, that is, the first depth zone with depth Z_1, are of concern.

The three force types (F_C, F_H and F_S) govern three modes of restoration mechanics, namely, depth impact, Hookean and tip-shape nanomechanics, respectively. The contributions (or strengths) of the three nanomechanics to the overall response are represented by the spring constants (k_C, k_H, k_S) of three parallel-connected spring (3PCS) analogs. The stiffness is defined as $k_T = k_H + k_S$. Another important elastic parameter is $r_S = k_S/k_T$, which quantifies penetration ease of the material and the composition of responding nanomechanics; it can represent material rigidity or deformability. Moreover, the F_S–deduced effective Young's modulus, $\hat{E} = E/(1 - \eta^2)$ with E the Young's modulus and η the Poisson's ratio, represents the intrinsic property of elasticity. The calculations of these parameters were detailed previously (Chen et al., 2023).

3 | RESULTS

To evaluate the relationship between root extension and root cell wall elasticity, we used AFM to perform vertical indentations on surfaces of living plant roots. We analyzed elastic responses of the CWs of Arabidopsis seedlings in the presence of metallic stresses, either Fe or Al alone or both combined. We used a robust measurement protocol to obtain reproducible and reliable results (Kaur, Teulon, et al., 2023). Seeds are sown on Day 0 on a 24-well crystallization plate, a key step that reduces the waving effect of seedling growth. On Day 4, seedlings are transferred on a 25 mm agar plate with or without metals (Fe, Al or Fe/Al) for 2 h. Then, seedlings are removed from the agar plates, deposited on a glass slide over a specific pressure sensitive adhesive (see Section 2), and quickly covered with growth media to avoid stress due to air exposure. Force-distance curves are measured using AFM. Because of the heterogeneity of seedling CW surfaces, we used the recently developed trimechanics-3PCS framework for interpreting force-distance curves (Chen et al., 2023). The trimechanics-3PCS framework allows the extraction of both stiffness and elasticity along the depth of indentation.

3.1 | WT seedling root lengths and elasticity in the absence of metals

The nonstressed (control) systems were characterized as the seedling roots grown without supplemented metals (Fe0Al0) with or without a

transfer step. In our nomenclature, metal stresses are given for both Fe and Al in μM; thus, Fe0Al0 indicates that 0 μM of $FeCl_2$ and 0 μM of $AlCl_3$ were added during the transfer step. Nanoindentation experiments were performed on these nonstressed seedlings 2 h later after being transferred, or immediately in case of no transfer. According to p values with the significance threshold $\alpha = 0.01$, no single group in the control systems significantly distinguishes itself from the others (Supporting Information S2: Figure 1). These results demonstrate that the transfer of seedlings do not alter the properties of the cell wall. In this work, negative control data includes only Fe0Al0 with the transfer step.

The average of root length obtained on Day 6 (4 days growth + 2 days after transferring from the Fe0Al0 condition) is 25.0 mm (Table 1). Averaged elasticity parameters are listed in Table 2. The results show that the effective Young modulus $\hat{E}$ for Fe0Al0 is about 54 kPa, the stiffness $k_T \sim 4.3\ 10^{-3}$ N/m, and indentation depth $Z_1 \sim 150$ nm.

3.2 | WT seedling root lengths and elasticity in the presence of metals

Several combinatory concentrations of Fe and Al were applied to the test on the growth and CW stiffening of seedling roots. Systematically, the seedling roots were placed under metal stress for 2 h. These stress conditions were prepared with 10 μM of $FeCl_2$ or 10 μM of $AlCl_3$, or mixing both, and labelled as Fe10Al0, Fe0Al10 and Fe10Al10, respectively. No REA is observed in either Fe0Al10 or Fe10Al0 whereas a full REA is observed in the Fe10Al10 condition (Figure 2a), see Table 1 for root lengths.

The results from nanoindentation experiments in 10 μM metal conditions are shown in Figure 2. The hierarchical averages of their elasticity parameters are presented in Table 2. The elastic behaviours of conditions Fe10Al0 and Fe0Al10 exhibit no distinction from Fe0Al0; with an average $\hat{E}$ of about 55 kPa. It indicates that the total amount of metal ions at 10 μM changes little in the effective Young's modulus, stiffness or indentation depth compared to no metal at all. However, the elasticity of roots grown with mixed Fe and Al (Fe10Al10) yields a value of 127 kPa for the effective Young's modulus $\hat{E}$, a significant increase in CW stiffness. However, although the averaged k_T of 8.89 10^{-3} N/m for Fe10Al10 is about double that of all the conditions of a single metal element at 10 μM (cf. 4–5 10^{-3} N/m in Table 2), there is no statistical significance likely due to the very large standard deviation for Fe10Al10 (Figure 2c).

We further explored the concentration impact of metal ions by doubling the concentration from 10 to 20 μM. We found that Fe20Al0 displays a significantly higher $\hat{E}$ and k_T than the control systems, while Fe0Al20 exhibits a moderate effect (Figure 2). The results show that the average of $\hat{E}$ and k_T have a similar value between Fe20Al0 and Fe10Al10 conditions (Table 2) whereas the corresponding values of Fe0Al20 are intermediate. Very interestingly, doubling the cationic concentration of single metal does not provoke the occurrence of REA (Table 1).

TABLE 1 The average of seedling root length for all study systems.

Plant type	Stress conditions	*n*	Length (mm)
WT	Fe0Al0	19	25.0 ± 3.1
	Fe0Al10	18	27.6 ± 3.1
	Fe10Al0	17	26.8 ± 3.3
	Fe10Al10	19	13.4 ± 1.3
	Fe0Al20	26	26.8 ± 2.8
	Fe20Al0	24	25.1 ± 2.2
	Fe10Al10+P	27	25.0 ± 2.9
almt1	ALMT1_Fe0Al0	9	23.5 ± 2.1
	ALMT1_Fe10Al10	9	22.0 ± 4.9

3.3 | *almt1* mutant seedling root lengths and elasticity in the presence of metals

Unlike WT seedling roots, no REA phenotype was found from *almt1* mutants in the Fe10Al10 condition (Table 1, Figure 3). The elasticity parameters for *almt1* mutant seedlings grown in Fe0Al0 and Fe10Al10 conditions are listed in Table 3. No significant difference was found in the magnitudes of $\hat{E}$ and k_T between the two stress conditions (Figure 3). Moreover, these values are comparable to WT in Fe0Al0 (Tables 2 and 3). This implies that without exuded malate

TABLE 2 Elastic properties of WT seedling roots.

	n	Z_1 (nm)	$\hat{E}$ (kPa)	r_S	k_T (10^{-3} N/m)
Fe0Al0	11	147 ± 55	53.9 ± 21.8	0.78 ± 0.05	4.30 ± 1.16
Fe0Al10	10	150 ± 62	51.7 ± 30.9	0.74 ± 0.07	4.26 ± 1.73
Fe10Al0	14	153 ± 41	58.4 ± 50.4	0.75 ± 0.08	4.94 ± 3.51
Fe10Al10	11	127 ± 57	105 ± 52	0.81 ± 0.09	8.89 ± 8.63
Fe0Al20	15	136 ± 41	76.9 ± 39.4	0.81 ± 0.05	5.72 ± 2.18
Fe20Al0	11	119 ± 29	106 ± 42	0.83 ± 0.06	7.51 ± 3.77
Fe10Al10+P	8	162 ± 25	59.6 ± 27.6	0.81 ± 0.06	5.37 ± 1.97

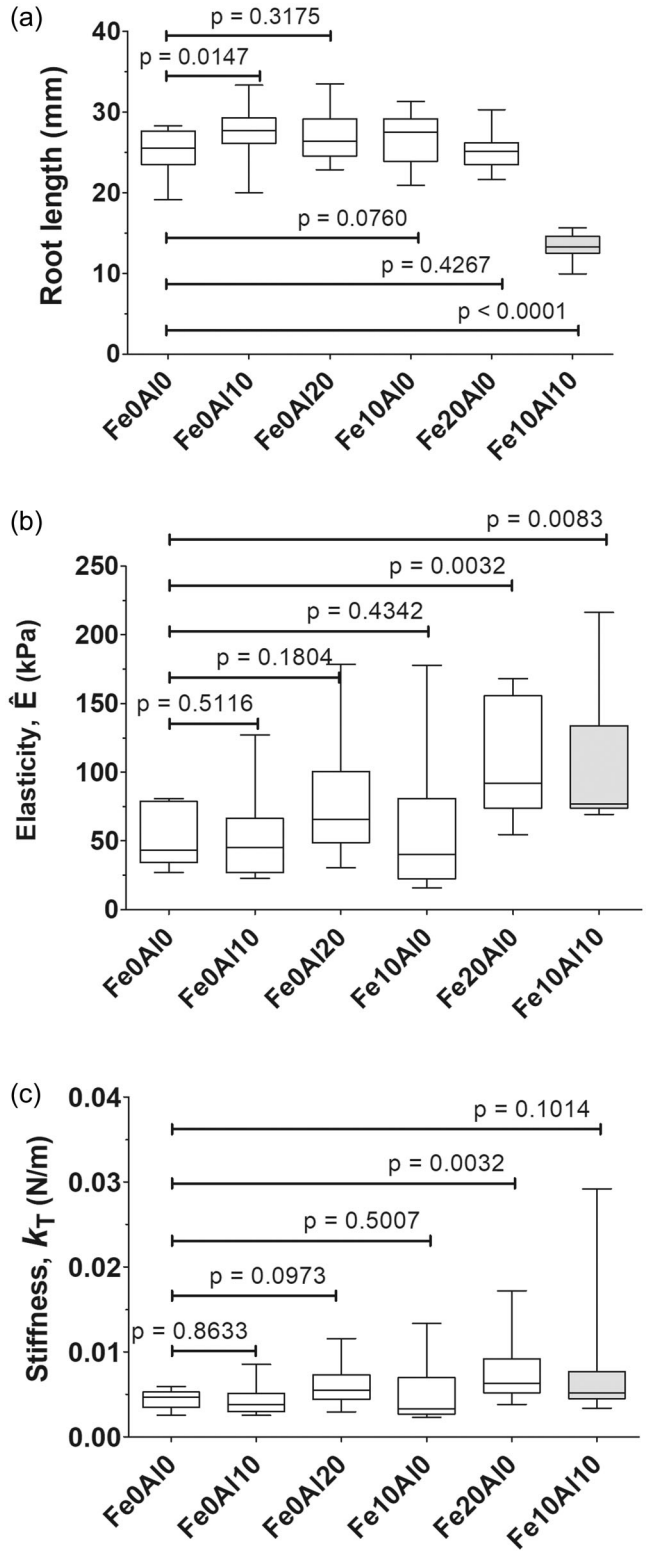

FIGURE 2 Box-and-whiskers plots of elastic parameters of WT seedling roots in various stress metal concentration. (a) Average root lengths measured on Day 6. (b) Effective Young's modulus ($\hat{E}$) in the kPa unit. (c) Stiffness measure, k_T, in the N/m unit.

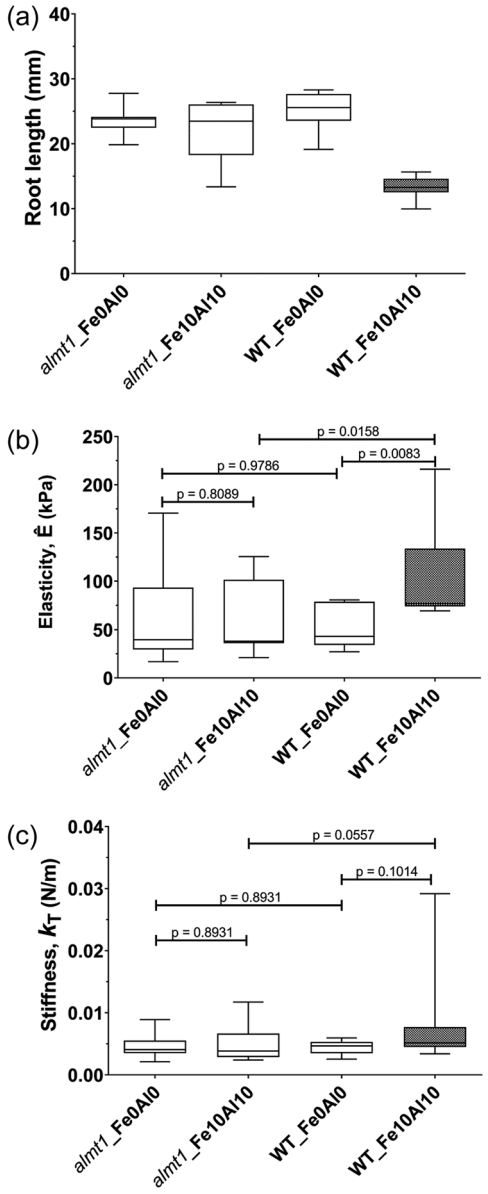

FIGURE 3 Box-and-whiskers plots of elastic properties of *almt1* mutant roots in comparison with WT (cf. Figure 2) in two stressed conditions, Fe0Al0 and Fe10Al10. (a) Average root lengths measured on Day 6. (b) Effective Young's modulus, $\hat{E}$, (in kPa). (c) Presentation of k_T in the N/m unit.

TABLE 3 Elastic properties of *almt1* mutant seedling roots.

	n	Z_1 (nm)	$\hat{E}$ (kPa)	r_S	k_T (10^{-3} N/m)
Fe0Al0	14	162 ± 79	63.5 ± 50.4	0.79 ± 0.08	4.6 ± 2.0
Fe10Al10	11	133 ± 28	58.3 ± 36.5	0.74 ± 0.08	4.8 ± 2.8

the two metal ions cannot exert substantial effects on elastic responses of mutant roots.

4 | DISCUSSION

The present results show that the elastic responses of external epidermal cell walls of Arabidopsis seedling roots to external forces vary in terms of concentration and composition of Fe and Al metal ions. It indicates that elasticity of plant CW is sensitive and can be used as to assess abiotic stresses on plant growth and stiffening. However, unexpectedly, the stiffening and the phenotype of seedling roots such as REA are not directly correlated.

4.1 | Root extension arrest (REA) and metallic stress

The root lengths of Arabidopsis seedlings were measured from the root tip to the cotyledon base (Supporting Information S2: Figure 2). Among all the stress conditions (Fe10Al0, Fe0Al10, Fe20Al0, Fe0Al20, and Fe10Al10), we observed the REA phenotype appeared only in the WT roots grown in the Fe10Al10 condition (Table 1). It is surprising that no REA was observed with doubled concentrations of single metal species (either Fe or Al). This reveals that the excess of a single metal species did not trigger the occurrence of REA. To ascertain that the REA phenotype is only due to the mixture of the two metal species, we carried out an experiment in a condition with the same metal ingredients and 500 μM phosphate (Pi). Phosphate is known for binding cations (Foy et al., 1978) but does not completely abolish the entry of metals into seedling roots (Balzergue et al., 2017). Results show no REA in the presence of Pi (Table 2, Supporting Information S2: Figure 5).

To further resolve the origin of REA occurrence, the WT results were compared with those of the *almt1* mutant. Lacking the malate-transporter ALMT1, the *almt1* mutant is strongly altered in exuding malate, a small organic anion known to chelate Fe^{3+} and Al^{3+}. The root growth of *almt1* mutant was known to be insensitive to Fe^{2+} (under −Pi condition) and exhibited no REA phenotype (Balzergue et al., 2017; Mora-Macias et al., 2017). The absence of REA phenotype was explained as a consequence of reduced accumulation of iron in the apoplast due to a dramatic decrease of malate exudation. From our results, the mixed Fe and Al stress also lacks the ability to stimulate REA in the *almt1* mutants, and these mixed metal cations act like single metal ions of 10 μM in WT roots. In other words, without the malate exudation, the mixed Al and Fe are no longer growth inhibitors, leading to a normal growth phenotype. It further suggests that trapping metal ions by malate molecules is a key step to promote REA in WT. Taken together, these data suggest that the factors to simulate REA include the amount of metal ions, the composition of metal species and the exudation of malate.

4.2 | Metallic stress and elasticity of living seedling roots

When the interlaced architecture of CWs is perturbed by metal ions, the bonding modes are accordingly adjusted; these changes can be reflected by altered elastic responses. It is noteworthy that the used AFM indenting tip has a small apex (~10 nm radius), enabling us to sense structural strengths of different layers of constituents in primary CWs such as cellulose microfibrils. Applying the trimechanic-3PCS framework to data analysis, the elasticity parameters defined therein helped us to differentiate elastic properties modulated by various stressed environments. The force decomposition of the theory reveals that the F_S-deduced $\hat{E}$ is a sensitive parameter to varying metal content in the growth medium (Table 2). The change in penetration ease r_S underlies the varying modes of nanomechanics and network bonding of CW architecture under different stresses (Chen et al., 2023). The r_S parameter is provided only by the trimechanic-3PCS framework and cannot be accessed by the conventional methods (Hermanowicz et al., 2014). This r_S parameter can also represent the deformability of the indented root.

According to comparable r_S values of WT roots in Fe0Al0, Fe10Al0 and Fe0Al10 conditions, the bonding properties of CW structure are inferred to be alike. However, with higher concentration of metal ions (Fe20Al0, Fe0Al20 and Fe10Al10), an increase in r_S is observed ($r_S > 0.8$, Table 2). It follows that in all these conditions of high metal concentration, the bonding properties of CW are different from that of low metal concentration. As already demonstrated, Al binds directly to negatively charged pectins of CWs and provokes a reduction in CW extensibility (Ma et al., 2004; Yang et al., 2016). In addition, expression profiling experiments suggested that pectins do bind with Fe (Hoehenwarter et al., 2016), which therefore, like Al, changes the bonding elasticity of the external primary cell wall. It is noteworthy that elastic parameters presented here are referred to the indentation depth of about 150 nm, which most likely corresponds to the pectin constituents of CW (as opposed to cellulose microfibrils). Thus, the increased stiffness of CW for seedlings grown from Fe20Al0 and Fe0Al20 conditions likely involves the binding of Fe and Al to the pectin components of CW.

From the results of Z_1, $\hat{E}$ or k_T, the increase of the total amount of metal ions is closely related to CW stiffening. At 10 μM of either iron or aluminum, the elastic properties of WT roots are similar to that of the control that contains no metal ions. At 20 μM (regardless of metal composition), the parameters $\hat{E}$, k_T and r_S increase while Z_1 slightly reduces; see the results from Fe10Al10, Fe20Al0 and Fe0Al20 in Table 2. However, the Fe20Al0 and Fe0Al20 (single metal species) conditions exhibit no REA phenotype. Thus, the increase of CW stiffness is not causal or not sufficient to trigger REA, at least not in the conditions of our experiments, that is, short-term treatment.

4.3 | Root extension arrest and CW stiffening

The REA phenotype induced by the Al stress is multifactorial and its mechanism remains largely unknown (Kochian et al., 2015). However,

from our previous work and others, the REA phenotype due to Fe stress is documented in its initial steps of Fe redox cycle that produces ROS in the CW and promotes peroxidase-dependent cell wall stiffening in the transition zone (Balzergue et al., 2017; Naumann et al., 2022). The major tolerance mechanism of Al toxicity is through the stimulation of the expression of the *ALMT1* gene (Godon et al., 2019), which encodes a malate transporter (ALMT1 [Sasaki et al., 2004]). The rate-limiting step in this mechanism is the transport of organic acids rather than the cellular synthesis of these molecules (Ryan et al., 2001). Indeed, Al^{3+} binding to the extracellular face of the ALMT1 channel opens the channel thereby stimulating the exudation of malate (Wang et al., 2022).

We have shown that the CW stiffness increases without REA at high Fe^{2+} concentrations (≥20 μM) for seedling roots grown from an agar medium with poor phosphate and other metals, probably reflecting a lack of ROS production (Figure 4). In the ferrous state, the Fe ion has multiple possible outcomes: adsorbed by the cell via its importing receptor, chelated with some organic acids in the CW or oxidized to a ferric ion that may nonspecifically bind to pectins of the CW. However, at 20 μM Fe^{2+}, none of these outcomes are important enough to form the necessary redox condition for REA occurrence. At the same concentration, Al^{3+} activates the exudation of malate that chelates Al to move it out of the root. It is known that Al^{3+} ions have a high affinity for pectic molecules of the cell wall and this binding is considered a major cause of Al^{3+} toxicity (Horst et al., 2010). Furthermore, within a few minutes Al^{3+} inhibits wall loosening in the elongation zone (Hajiboland et al., 2023). The Al^{3+} ions unbound to malate molecules in the CW then bind to negatively-charged pectins, leading to an increase of stiffness though without REA occurrence (Figure 4). The stress effect of the co-presence of Fe and Al highlights the importance of malate accumulated in the apoplast. A current model postulates that, in combination with the apoplastic ferroxidase LPR1, malate-Fe^{3+} complexes trigger ROS in the apoplast (Naumann et al., 2022). Based on this model, our results show that Al^{3+} increases exudation of malate in the apoplast, thereby accumulating Fe in the apoplast followed by an accumulation of ROS to end up with a root extension arrest (Figure 4).

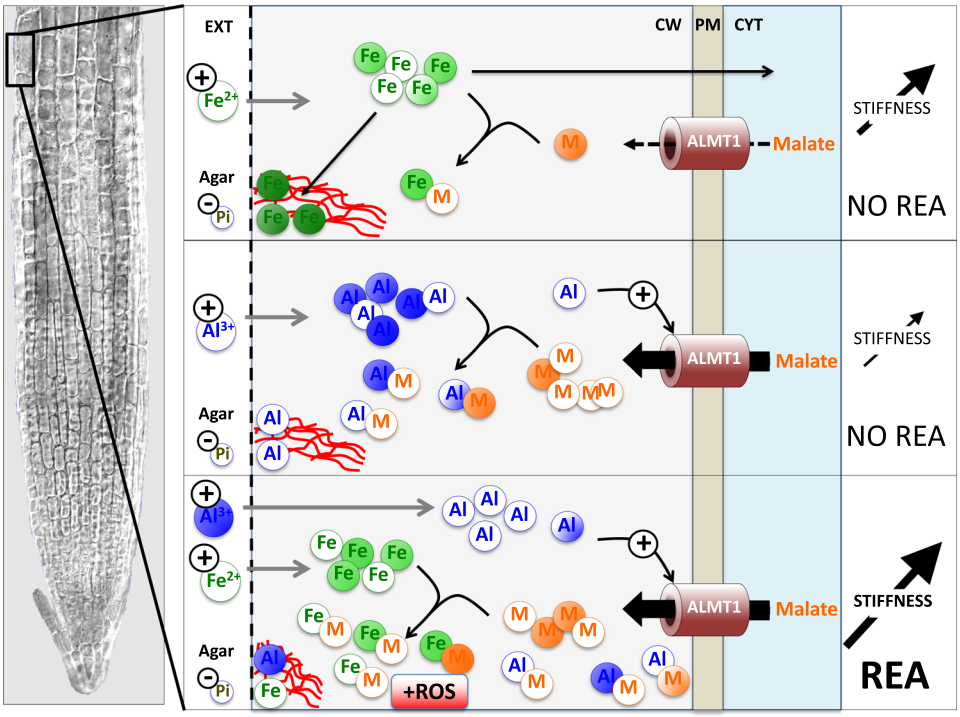

FIGURE 4 Model explaining the effects of Fe and Al on CW stiffening and root extension. Left panel shows a reconstituted picture of an Arabidopsis primary root tip; the square indicates part of the epidermis in the transition zone, where AFM measures were performed in this work. The top to bottom panels explain the phenomena that occur, depending on the Fe^{2+} and Al^{3+} content of the Pi-poor culture medium. Top panel: the Fe^{2+} ions enter the apoplast of the cell wall (CW, in light grey background colour), which subsequently can cross the plasma membrane (PM, in light tan colour) through an unknown transporter (not presented here for clarity) and activates the STOP1-ALMT1 signalling (not shown), or accumulate into the apoplast in complex with constitutively present small organic acids like malate (M). The ALMT1 transporter exports malate from the cytosol (CYT, light blue background) to the apoplast. The accumulation of Fe cations, possibly in the Fe^{3+} state (darker green on the bottom left) binds to pectins (curled red lines), thereby increasing CW stiffness without triggering the root extension arrest (REA). Middle panel: the Al^{3+} ions enter the CW and activate the transcription of *ALMT1* (not shown) and the opening of ALMT1 transporter, thereby releasing malate in the apoplast. The accumulation of Al^{3+} leads to a modest increase of CW stiffness mostly of pectins, but without REA. Bottom panel: the combination of Fe^{2+} and Al^{3+} results in a large release of malate and a high accumulation of ROS-promoting iron-malate complexes in the apoplast. These ROS concomitantly increase CW stiffness (besides the effect of metals on pectins) and strongly prevents root extension. CW, cell wall; CYT, cytoplasm; M, malate; PM, plasma membrane; REA, root extension arrest; −Pi, phosphate-poor medium; +Fe, adding Fe^{2+} in the medium; +Al, adding Al^{3+} in the medium. [Color figure can be viewed at wileyonlinelibrary.com]

Our AFM study shows that aluminum acts rapidly on parietal stiffness and the synergy with iron amplifies this inhibition. These results provide a better understanding of the interaction of iron and aluminum found in acidic soils. This work is a step forward to decipher the interplay of metal bioavailability in low phosphate conditions. It may also provide future route to develop and grow breeding targets best adapted to Al^{3+} stress.

5 | CONCLUSIONS

Root extension arrest was observed from *A. thaliana* WT seedlings only stressed by a mix of 10 µM $FeCl_2$ and 10 µM $AlCl_3$ in a low phosphate agar medium. This REA is concomitant with a stiffening of the external primary cell walls. However, single metals, even at a higher concentration (20 µM), did not induce REA despite an increase in CW stiffness. Thus, the increase in the stiffness of CW may have independent origins: one associated with the binding of metals to pectin components of CW, and another associated with the redox cycle that produces ROS in the CW and promotes the peroxidase-dependent stiffening of CW. Consequently, the REA occurs in a balance of metabolic events (chemical and/or mechanical) that depends upon a change in the contribution of each factors including the chelating effect of malate in the combined Fe-Al stress.

ACKNOWLEDGEMENTS

IBS acknowledges integration into the Interdisciplinary Research Institute of Grenoble (IRIG, CEA). This work acknowledges the AFM platform at the IBS. Acknowledgement to the ANR project BioPhyt –18-CE20-0023-03 and the support of the European Union's Horizon 2020 research and innovation programme under the Marie Skłodowska-Curie grant agreement No 812772, Project Phys2-BioMed. We thank Dr. Anne-Emmanuelle Foucher (IBS/EPIGEN) for critical improvements of the plant growth protocol. We also thank Isabel Ayala and Lionel Imbert (IBS/NMR) for their support in lab experiments. We are grateful to Chloe Zubieta for improving the manuscript.

DATA AVAILABILITY STATEMENT

Data available on request from the authors.

ORCID

Harinderbir Kaur http://orcid.org/0000-0002-2418-2449
Christian Godon http://orcid.org/0000-0002-1535-9855
Thierry Desnos http://orcid.org/0000-0002-6585-1362
Shu-wen W. Chen http://orcid.org/0000-0003-4205-4931
Jean-Luc Pellequer http://orcid.org/0000-0002-8944-2715

REFERENCES

Abel, S. (2011) Phosphate sensing in root development. *Current Opinion in Plant Biology*, 14(3), 303–309. Available from: https://doi.org/10.1016/j.pbi.2011.04.007

Balzergue, C., Dartevelle, T., Godon, C., Laugier, E., Meisrimler, C., Teulon, J.-M. et al. (2017) Low phosphate activates STOP1-ALMT1 to rapidly inhibit root cell elongation. *Nature Communications*, 8, 15300. Available from: https://doi.org/10.1038/ncomms15300

Bashline, L., Lei, L., Li, S. & Gu, Y. (2014) Cell wall, cytoskeleton, and cell expansion in higher plants. *Molecular Plant*, 7(4), 586–600. Available from: https://doi.org/10.1093/mp/ssu018

Bauer, W.D., Talmadge, K.W., Keegstra, K. & Albersheim, P. (1973) The structure of plant cell walls: II. The hemicellulose of the walls of suspension-cultured sycamore cells. *Plant Physiology*, 51(1), 174–187. Available from: https://doi.org/10.1104/pp.51.1.174

Bian, M., Zhou, M., Sun, D. & Li, C. (2013) Molecular approaches unravel the mechanism of acid soil tolerance in plants. *The Crop Journal*, 1, 91–104. Available from: https://doi.org/10.1016/j.cj.2013.08.002

Bidhendi, A.J. & Geitmann, A. (2016) Relating the mechanics of the primary plant cell wall to morphogenesis. *Journal of Experimental Botany*, 67(2), 449–461. Available from: https://doi.org/10.1093/jxb/erv535

Bienfait, H.F., Vandenbriel, W. & Meslandmul, N.T. (1985) Free space iron pools in roots—generation and mobilization. *Plant Physiology*, 78(3), 596–600. Available from: https://doi.org/10.1104/pp.78.3.596

Bonnot, C., Pinson, B., Clément, M., Bernillon, S., Chiarenza, S., Kanno, S. et al. (2016) A chemical genetic strategy identify the PHOSTIN, a synthetic molecule that triggers phosphate starvation responses in *Arabidopsis thaliana*. *New Phytologist*, 209(1), 161–176. Available from: https://doi.org/10.1111/nph.13591

Cakmak, I. & Horst, W.J. (1991) Effect of aluminium on lipid peroxidation, superoxide dismutase, catalase, and peroxidase activities in root tips of soybean (*Glycine max*). *Physiologia Plantarum*, 83, 463–468. Available from: https://doi.org/10.1111/j.1399-3054.1991.tb00121.x

Carpita, N.C. & Gibeaut, D.M. (1993) Structural models of primary cell walls in flowering plants: consistency of molecular structure with the physical properties of the walls during growth. *The Plant Journal*, 3(1), 1–30.

Chang, Y.-C., Yamamoto, Y. & Matsumoto, H. (1999) Accumulation of aluminium in the cell wall pectin in cultured tobacco (*Nicotiana tabacum* L.) cells treated with a combination of aluminium and iron. *Plant, Cell & Environment*, 22, 1009–1017. Available from: https://doi.org/10.1046/j.1365-3040.1999.00467.x

Chen, S.W., Teulon, J.M., Kaur, H., Godon, C. & Pellequer, J.L. (2023) Nano-structural stiffness measure for soft biomaterials of heterogeneous elasticity. *Nanoscale Horizons*, 8, 75–82. Available from: https://doi.org/10.1039/D2NH00390B

Clarkson, D.T. (1965) The effect of aluminium and some other trivalent metal cations on cell division in the root apices of *Allium cepa*. *Annals of Botany*, 29(114), 309–315. Available from: https://doi.org/10.1093/oxfordjournals.aob.a083953

Cosgrove, D.J. (1997) Relaxation in a high-stress environment: the molecular bases of extensible cell walls and cell enlargement. *The Plant Cell*, 9(7), 1031–1041. Available from: https://doi.org/10.1105/tpc.9.7.1031

Cosgrove, D.J. (2005) Growth of the plant cell wall. *Nature Reviews Molecular Cell Biology*, 6(11), 850–861. Available from: https://doi.org/10.1038/nrm1746

Cosgrove, D.J. (2018) Nanoscale structure, mechanics and growth of epidermal cell walls. *Current Opinion in Plant Biology*, 46, 77–86. Available from: https://doi.org/10.1016/j.pbi.2018.07.016

Cuadrado-Pedetti, M.B., Rauschert, I., Sainz, M.M., Amorim-Silva, V., Botella, M.A., Borsani, O. et al. (2021) The Arabidopsis TETRATRICOPEPTIDE THIOREDOXIN-LIKE 1 gene is involved in anisotropic root growth during osmotic stress adaptation. *Genes*, 12(2), 236. Available from: https://doi.org/10.3390/genes12020236

Delhaize, E. & Ryan, P.R. (1995) Aluminum toxicity and tolerance in plants. *Plant Physiology*, 107(2), 315–321. Available from: https://doi.org/10.1104/pp.107.2.315

Delhaize, E., Ryan, P.R. & Randall, P.J. (1993) Aluminum tolerance in wheat (*Triticum aestivum* L.) (II. Aluminum-stimulated excretion of malic acid from root apices). *Plant Physiology*, 103(3), 695–702. Available from: https://doi.org/10.1104/pp.103.3.695

Derbyshire, P., Findlay, K., McCann, M.C. & Roberts, K. (2007) Cell elongation in Arabidopsis hypocotyls involves dynamic changes in cell wall thickness. *Journal of Experimental Botany*, 58(8), 2079–2089. Available from: https://doi.org/10.1093/jxb/erm074

Foy, C.D., Chaney, R.L. & White, M.C. (1978) The physiology of metal toxicity in plants. *Annual Review of Plant Physiology*, 29, 511–566. Available from: https://doi.org/10.1146/annurev.pp.29.060178.002455

Francoz, E., Ranocha, P., Nguyen-Kim, H., Jamet, E., Burlat, V. & Dunand, C. (2015) Roles of cell wall peroxidases in plant development. *Phytochemistry*, 112, 15–21. Available from: https://doi.org/10.1016/j.phytochem.2014.07.020

Gaff, D. & Carr, D. (1961) The quantity of water in the cell wall and its significance. *Australian Journal of Biological Sciences*, 14(3), 299–311. Available from: https://doi.org/10.1071/Bi9610299

Gill, S.S. & Tuteja, N. (2010) Reactive oxygen species and antioxidant machinery in abiotic stress tolerance in crop plants. *Plant Physiology and Biochemistry*, 48(12), 909–930. Available from: https://doi.org/10.1016/j.plaphy.2010.08.016

Godon, C., Mercier, C., Wang, X., David, P., Richaud, P., Nussaume, L. et al. (2019) Under phosphate starvation conditions, Fe and Al trigger accumulation of the transcription factor STOP1 in the nucleus of Arabidopsis root cells. *The Plant Journal*, 99(5), 937–949. Available from: https://doi.org/10.1111/tpj.14374

Hajiboland, R., Panda, C.K., Lastochkina, O., Gavassi, M.A., Habermann, G. & Pereira, J.F. (2023) Aluminum toxicity in plants: present and future. *Journal of Plant Growth Regulation*, 42, 3967–3999.

Hermanowicz, P., Sarna, M., Burda, K. & Gabryś, H. (2014) AtomicJ: an open source software for analysis of force curves. *Review of Scientific Instruments*, 85(6), 063703. Available from: https://doi.org/10.1063/1.4881683

Hirsch, J., Marin, E., Floriani, M., Chiarenza, S., Richaud, P., Nussaume, L. et al. (2006) Phosphate deficiency promotes modification of iron distribution in Arabidopsis plants. *Biochimie*, 88(11), 1767–1771. Available from: https://doi.org/10.1016/j.biochi.2006.05.007

Hoehenwarter, W., Mönchgesang, S., Neumann, S., Majovsky, P., Abel, S. & Müller, J. (2016) Comparative expression profiling reveals a role of the root apoplast in local phosphate response. *BMC Plant Biology*, 16, 106. Available from: https://doi.org/10.1186/s12870-016-0790-8

Horst, W.J., Wang, Y. & Eticha, D. (2010) The role of the root apoplast in aluminium-induced inhibition of root elongation and in aluminium resistance of plants: a review. *Annals of Botany*, 106(1), 185–197. Available from: https://doi.org/10.1093/aob/mcq053

Jackman, R.L. & Stanley, D.W. (1995) Perspectives in the textural evaluation of plant foods. *Trends in Food Science & Technology*, 6(6), 187–194. Available from: https://doi.org/10.1016/S0924-2244(00)89053-6

Kaur, H., Godon, C., Teulon, J.-M., Desnos, T. & Pellequer, J.-L. (2023) Preparation and deposition of plant roots for AFM nanomechanical measurements. In: Lekka, M., Navajas, D., Radmacher, M. & Podestà, A. (Eds.) *Mechanics of cells and tissues in diseases*, 2. Berlin/Boston: Walter de Gruyter GmbH, pp. 125–138.

Kaur, H., Teulon, J.-M., Foucher, A.-E., Fenel, D., Chen, S.W., Godon, C. et al. (2023) Measuring external primary cell wall elasticity of seedling roots using atomic force microscopy. *STAR Protocols*, 4, 102265. Available from: https://doi.org/10.1016/j.xpro.2023.102265

Kerr, T. & Bailey, I.W. (1934) The cambium and its derivative tissues: no. X. Structure, optical properties and chemical composition of the so-called middle lamella. *Journal of the Arnold Arboretum*, 15, 327–349. Available from: http://www.biodiversitylibrary.org/item/33591

Kierzkowski, D., Nakayama, N., Routier-Kierzkowska, A.L., Weber, A., Bayer, E., Schorderet, M. et al. (2012) Elastic domains regulate growth and organogenesis in the plant shoot apical meristem. *Science*, 335(6072), 1096–1099. Available from: https://doi.org/10.1126/science.1213100

Kochian, L.V., Piñeros, M.A., Liu, J. & Magalhaes, J.V. (2015) Plant adaptation to acid soils: the molecular basis for crop aluminum resistance. *Annual Review of Plant Biology*, 66, 571–598. Available from: https://doi.org/10.1146/annurev-arplant-043014-114822

Kutschera, U. (1996) Cessation of cell elongation in rye coleoptiles is accompanied by a loss of cell-wall plasticity. *Journal of Experimental Botany*, 47(302), 1387–1394. Available from: https://doi.org/10.1093/jxb/47.9.1387

Liu, J., Magalhaes, J.V., Shaff, J. & Kochian, L.V. (2009) Aluminum-activated citrate and malate transporters from the MATE and ALMT families function independently to confer Arabidopsis aluminum tolerance. *The Plant Journal*, 57(3), 389–399. Available from: https://doi.org/10.1111/j.1365-313X.2008.03696.x

Ma, J.F., Shen, R., Nagao, S. & Tanimoto, E. (2004) Aluminum targets elongating cells by reducing cell wall extensibility in wheat roots. *Plant and Cell Physiology*, 45(5), 583–589. Available from: https://doi.org/10.1093/pcp/pch060

MacAdam, J. & Grabber, J. (2002) Relationship of growth cessation with the formation of diferulate cross-links and p-coumaroylated lignins in tall fescue leaf blades. *Planta*, 215(5), 785–793. Available from: https://doi.org/10.1007/s00425-002-0812-7

Macara, I.G., Hoy, T.G. & Harrison, P.M. (1972) The formation of ferritin from apoferritin. *Biochemical Journal*, 126(1), 151–162. Available from: https://doi.org/10.1042/bj1260151

Majda, M., Grones, P., Sintorn, I.M., Vain, T., Milani, P., Krupinski, P. et al. (2017) Mechanochemical polarization of contiguous cell walls shapes plant pavement cells. *Developmental Cell*, 43(3), 290–304. Available from: https://doi.org/10.1016/j.devcel.2017.10.017

McCann, M.C., Wells, B. & Roberts, K. (1990) Direct visualization of cross-links in the primary plant cell wall. *Journal of Cell Science*, 96, 323–334. Available from: https://doi.org/10.1242/jcs.96.2.323

Meijering, E., Jacob, M., Sarria, J.C.F., Steiner, P., Hirling, H. & Unser, M. (2004) Design and validation of a tool for neurite tracing and analysis in fluorescence microscopy images. *Cytometry, Part A*, 58(2), 167–176. Available from: https://doi.org/10.1002/cyto.a.20022

Mercier, C., Roux, B., Have, M., Le Poder, L., Duong, N., David, P. et al. (2021) Root responses to aluminium and iron stresses require the SIZ1 SUMO ligase to modulate the STOP1 transcription factor. *The Plant Journal*, 108(5), 1507–1521. Available from: https://doi.org/10.1111/tpj.15525

Milani, P., Gholamirad, M., Traas, J., Arnéodo, A., Boudaoud, A., Argoul, F. et al. (2011) In vivo analysis of local wall stiffness at the shoot apical meristem in Arabidopsis using atomic force microscopy. *The Plant Journal*, 67(6), 1116–1123. Available from: https://doi.org/10.1111/j.1365-313X.2011.04649.x

Milani, P., Mirabet, V., Cellier, C., Rozier, F., Hamant, O., Das, P. et al. (2014) Matching patterns of gene expression to mechanical stiffness at cell resolution through quantitative tandem epifluorescence and nanoindentation. *Plant Physiology*, 165(4), 1399–1408. Available from: https://doi.org/10.1104/pp.114.237115

Miyasaka, S.C., Buta, J.G., Howell, R.K. & Foy, C.D. (1991) Mechanism of aluminum tolerance in snapbeans: root exudation of citric acid. *Plant Physiology*, 96(3), 737–743. Available from: https://doi.org/10.1104/pp.96.3.737

Mora-Macias, J., Ojeda-Rivera, J.O., Gutierrez-Alanis, D., Yong-Villalobos, L., Oropeza-Aburto, A. & Raya-Gonzalez, J. (2017)

Malate-dependent Fe accumulation is a critical checkpoint in the root developmental response to low phosphate. *Proceedings of the National Academy of Sciences of the USA*, 114(17), E3563–E3572. https://doi.org/10.1073/pnas.1701952114

Müller, J., Toev, T., Heisters, M., Teller, J., Moore, K.L., Hause, G. et al. (2015) Iron-dependent callose deposition adjusts root meristem maintenance to phosphate availability. *Developmental Cell*, 33(2), 216–230. Available from: https://doi.org/10.1016/j.devcel.2015.02.007

Naumann, C., Heisters, M., Brandt, W., Janitza, P., Alfs, C., Tang, N. et al. (2022) Bacterial-type ferroxidase tunes iron-dependent phosphate sensing during Arabidopsis root development. *Current Biology*, 32(10), 2189–2205. Available from: https://doi.org/10.1016/j.cub.2022.04.005

Nichol, B.E., Oliveira, L.A., Glass, A. & Siddiqi, M.Y. (1993) The effects of aluminum on the influx of calcium, potassium, ammonium, nitrate, and phosphate in an aluminum-sensitive cultivar of barley (*Hordeum vulgare* L.). *Plant Physiology*, 101, 1263–1266. Available from: https://doi.org/10.1104/pp.101.4.1263

Oliveira de Araujo, T., Isaure, M.P., Alchoubassi, G., Bierla, K., Szpunar, J., Trcera, N. et al. (2020) *Paspalum urvillei* and *Setaria parviflora*, two grasses naturally adapted to extreme iron-rich environments. *Plant Physiology and Biochemistry*, 151, 144–156. Available from: https://doi.org/10.1016/j.plaphy.2020.03.014

Passardi, F., Cosio, C., Penel, C. & Dunand, C. (2005) Peroxidases have more functions than a Swiss army knife. *Plant Cell Reports*, 24(5), 255–265. Available from: https://doi.org/10.1007/s00299-005-0972-6

Peaucelle, A., Braybrook, S.A., Le Guillou, L., Bron, E., Kuhlemeier, C. & Höfte, H. (2011) Pectin-induced changes in cell wall mechanics underlie organ initiation in Arabidopsis. *Current Biology*, 21(20), 1720–1726. Available from: https://doi.org/10.1016/j.cub.2011.08.057

Le Poder, L., Mercier, C., Février, L., Duong, N., David, P. & Pluchon, S. et al. (2022) Uncoupling aluminum toxicity from aluminum signals in the STOP1 pathway. *Frontiers in Plant Science*, 13, 785791. Available from: https://doi.org/10.3389/fpls.2022.785791

Preston, R.D. & Hepton, J. (1960) The effect of indoleacetic acid on cell wall extensibility in Avena coleoptiles. *Journal of Experimental Botany*, 11(31), 13–27. Available from: https://doi.org/10.1093/Jxb/11.1.13

Ravet, K., Touraine, B., Boucherez, J., Briat, J.F., Gaymard, F. & Cellier, F. (2009) Ferritins control interaction between iron homeostasis and oxidative stress in Arabidopsis. *The Plant Journal*, 57(3), 400–412. Available from: https://doi.org/10.1111/j.1365-313X.2008.03698.x

Ryan, P., Delhaize, E. & Jones, D. (2001) Function and mechanism of organic anion exudation from plant roots. *Annual Review of Plant Physiology and Plant Molecular Biology*, 52, 527–560. Available from: https://doi.org/10.1146/annurev.arplant.52.1.527

Sasaki, T., Yamamoto, Y., Ezaki, B., Katsuhara, M., Ahn, S.J., Ryan, P.R. et al. (2004) A wheat gene encoding an aluminum-activated malate transporter. *The Plant Journal*, 37(5), 645–653. Available from: https://doi.org/10.1111/j.1365-313x.2003.01991.x

Schillers, H., Rianna, C., Schäpe, J., Luque, T., Doschke, H., Wälte, M. et al. (2017) Standardized nanomechanical atomic force microscopy procedure (SNAP) for measuring soft and biological samples. *Scientific Reports*, 7, 5117. Available from: https://doi.org/10.1038/s41598-017-05383-0

Schneider, C.A., Rasband, W.S. & Eliceiri, K.W. (2012) NIH image to ImageJ: 25 years of image analysis. *Nature Methods*, 9(7), 671–675. Available from: https://doi.org/10.1038/nmeth.2089

Schopfer, P. (2006) Biomechanics of plant growth. *American Journal of Botany*, 93(10), 1415–1425. Available from: https://doi.org/10.3732/ajb.93.10.1415

Somssich, M., Khan, G.A. & Persson, S. (2016) Cell wall heterogeneity in root development of Arabidopsis. *Frontiers in Plant Science*, 07, 1242. Available from: https://doi.org/10.3389/fpls.2016.01242

Svistoonoff, S., Creff, A., Reymond, M., Sigoillot-Claude, C., Ricaud, L., Blanchet, A. et al. (2007) Root tip contact with low-phosphate media reprograms plant root architecture. *Nature Genetics*, 39(6), 792–796. Available from: https://doi.org/10.1038/ng2041

Uddin, M.N., Hanstein, S., Faust, F., Eitenmüller, P.T., Pitann, B. & Schubert, S. (2014) Diferulic acids in the cell wall may contribute to the suppression of shoot growth in the first phase of salt stress in maize. *Phytochemistry*, 102, 126–136. Available from: https://doi.org/10.1016/j.phytochem.2014.02.014

Valent, B.S. & Albersheim, P. (1974) The structure of plant cell walls: v. On the binding of xyloglucan to cellulose fibers. *Plant Physiology*, 54(1), 105–108. Available from: https://doi.org/10.1104/pp.54.1.105

Wakabayashi, K., Soga, K. & Hoson, T. (2012) Phenylalanine ammonia-lyase and cell wall peroxidase are cooperatively involved in the extensive formation of ferulate network in cell walls of developing rice shoots. *Journal of Plant Physiology*, 169(3), 262–267. Available from: https://doi.org/10.1016/j.jplph.2011.10.002

Wang, J., Yu, X., Ding, Z.J., Zhang, X., Luo, Y., Xu, X. et al. (2022) Structural basis of ALMT1-mediated aluminum resistance in Arabidopsis. *Cell Research*, 32(1), 89–98. Available from: https://doi.org/10.1038/s41422-021-00587-6

Ward, J.T., Lahner, B., Yakubova, E., Salt, D.E. & Raghothama, K.G. (2008) The effect of iron on the primary root elongation of Arabidopsis during phosphate deficiency. *Plant Physiology*, 147(3), 1181–1191. Available from: https://doi.org/10.1104/pp.108.118562

Wissemeier, A.H., Diening, A., Hergenröder, A., Horst, W.J. & Mixwagner, G. (1992) Callose formation as parameter for assessing genotypical plant tolerance of aluminium and manganese. *Plant and Soil*, 146(1–2), 67–75. Available from: https://doi.org/10.1007/Bf00011997

Wolf, S. & Höfte, H. (2014) Growth control: A saga of cell walls, ROS, and peptide receptors. *The Plant Cell*, 26(5), 1848–1856. Available from: https://doi.org/10.1105/tpc.114.125518

Yang, J., Qu, M., Fang, J., Shen, R.F., Feng, Y.M., Liu, J.Y. et al. (2016) Alkali-soluble pectin is the primary target of aluminum immobilization in root border cells of pea (*Pisum sativum*. *Frontiers in Plant Science*, 7, 1297. Available from: https://doi.org/10.3389/fpls.2016.01297

SUPPORTING INFORMATION

Additional supporting information can be found online in the Supporting Information section at the end of this article.

How to cite this article: Kaur, H., Teulon, J.-M., Godon, C., Desnos, T., Chen, S.-w. W. & Pellequer, J.-L. (2023) Correlation between plant cell wall stiffening and root extension arrest phenotype in the combined abiotic stress of Fe and Al. *Plant, Cell & Environment*, 1–11. https://doi.org/10.1111/pce.14744